Energy and Environmental Engineering 2(7): 145-152, 2014 http://www.hrpub.org
DOI: 10.13189/eee.2014.020702

Evaluation of Model for Air Pollution in the Vicinity of Roadside Solid Barriers

Desmond Adair[1,*], Martin Jaeger[2]

[1]School of Engineering, Nazarbayev University, Republic of Kazakhstan
[2]School of Engineering & ICT, University of Tasmania, Australia

Abstract Roadside noise barriers and solid fences are common features along major highways in urban regions of Kazakhstan and are anticipated to have important effects on near-road air pollution through altering the dispersion of traffic emissions and resulting downstream concentrations. A 3-dimensional computational fluid dynamics (CFD) road model has been developed to simulate roadside barrier effects on near-road air quality and evaluate the influence of key variables, such as barrier height and wind direction. The CFD model is tested against experimental data and other existing models found in the literature, with several turbulence models tested to give optimal results, i.e., the standard $k-\varepsilon$ model and the realizable $k-\varepsilon$ model with different Schmidt numbers. The dispersion of a mixture of nitrogen oxides (denoted as NO_x—a mix of NO and NO_2) was computed and the barriers were assumed to be straight and infinitely long. Dispersion of NO_x was modeled for situations with no barriers along the highway, barriers on both sides, and for a single barrier on the downwind side of the highway. The modelling results are presented and discussed in relation to previous studies and the implications of the results are considered for pollution barriers along highways.

Keywords CFD Modelling, Roadside Barriers, Near-road Air Pollution

1. Introduction

In a recent study [1] it was concluded that in general, air pollution in Kazakhstan constitutes a significant contribution to the burden of diseases. In relative terms, the impact of air pollution on premature mortality in Kazakhstan is notably higher than in say Russia or the Ukraine. To add to this, public health concerns related to near-road air quality have become a pressing issue, due to the increasing number of epidemiological studies suggesting that populations spending significant amounts of time near heavily trafficked roads are at greater risk of adverse health effects [2,3]. Emission control techniques and programs are used to directly reduce emitted air pollutants and are an essential part of air quality management, but other strategies such as the planting of trees and bushes and the erection of road-side structures such as noise barriers are used as near-term mitigation strategies. Many roadside solid fences are also erected to hide unsightly building sites, etc. within urban areas in Kazakhstan. These methods, if successful, can provide measures to reduce impacts from sources that are difficult to mitigate [4].

Cars are responsible for high concentrations of both gaseous air pollution and particulates. Nitrogen oxides (NO and NO_2) are the most important of the many air pollution agents that are emitted into the atmosphere. Although the concentration of air pollutants is usually measured, there are a limited number of monitoring stations within a city. Therefore, the spatial distribution of these agents is often modeled rather than measured, particularly for city management and municipal authorities. Many cities use software such as the ADMS-Urban [5] or Gaussian-plume [6] software. Such systems (and others used in Europe and the USA) are used to model concentrations over whole or large parts of cities. In contrast, this study will focus on issues at a local level in close proximity to busy roads and streets in settled areas on the outskirts of large cities. These areas are typically densely populated, with large groups of houses protected from traffic noise by barriers and have solid fences erected for privacy or aesthetic uses.

Field studies have quantified steep spatial concentration gradients of traffic-related pollutants (e.g., carbon monoxide, ultrafine particles, black carbon, oxides of nitrogen), with a maximum concentration occurring next to the road and dropping exponentially to background levels within several hundred meters of a major roadway [7-10]. Traffic emissions have been linked to an exposure region of up to 300 - 500 m from the road. Also, several wind tunnel, numerical models, and field studies have indicated that roadside obstructions to air flow, such as tree stands or noise barriers, may have significant effects on vehicular emissions dispersion and ambient air pollutant

concentrations [11-14]. A study in California determined lower pollution levels in the lee of a barrier, relative to a clearing, but that concentrations rose to levels above the clearing further downwind [14] while a field experiment studying the dispersion of a sulphur hexiflouride (SF6) line source upwind of a 6 m high straw bale barrier, constructed to simulate a solid noise barrier, found concentration reductions downwind of the barrier relative to concentrations from the same source in a clearing, for a range of meteorological stability categories [13]. Wind tunnel experiments also show that for crosswind conditions, a roadside barrier leads to a vertical lofting of the roadway emissions and decrease of ground-level concentrations in the wake of a barrier, relative to a no-barrier case [12]. However, despite all these many works, there is still little information of how solid barriers affect pollutant transport, especially under a variety of barrier height and configurations [15]. Also the extent to which double barriers can reduce air pollution near roads, under varying noise-barrier heights remains uncertain [3].

The simulation of the dispersion of air pollution in complex situations, such as in the vicinity of roadside barriers, is difficult, but it has been suggested that progress can be made by building and running models using computational fluid dynamics (CFD) [16]. Therefore, in this work, in order to further understand the conditions that favor or disfavor air quality improvement by roadside barriers, a computational fluid dynamics (CFD) roadside barrier model was developed and tested against experimental results and other recent studies found in the literature.

2. CFD Model

A CFD model has been developed to simulate wind flow and pollutant concentration around both single and double solid roadside barriers. The simulations are based on Reynolds-averaged Navier-Stokes equations (RANS) using closure turbulence models, i.e. the standard $k-\varepsilon$ model [17] and the realizable $k-\varepsilon$ model [18], where k is the turbulent kinetic energy and ε is the dissipation rate of turbulence kinetic energy.

The continuity and momentum equations for incompressible fluid used are,

$$\frac{\partial u_i}{\partial x_j} = 0 \tag{1}$$

$$\frac{\partial u_i}{\partial t} + u_j \frac{\partial u_i}{\partial x_j} = -\frac{1}{\rho}\frac{\partial p}{\partial x_i} + \nu \frac{\partial^2 u_i}{\partial x_j \partial x_j} - \frac{\partial}{\partial x_j}\left(\overline{u_i' u_j'}\right) + g \tag{2}$$

where, u_i is the j^{th} component of velocity, t is the time, x_j is the j^{th} coordinate, ρ is the air density, υ is the kinematic viscosity, and g is the gravitational body force. The equation,

$$\overline{-u_i' u_j'} = \nu_t \left(\frac{\partial u_i}{\partial x_j} + \frac{\partial u_j}{\partial x_i}\right) - \frac{2}{3} k \delta_{ij} \tag{3}$$

is the Reynolds stress equation, where $\nu_t = C_\mu k^2/\varepsilon$ is the turbulent viscosity.

Enlarged-viscosity models became popular in the late 1970's due to development of the first computers, and rudiments of CFD programs, which allowed the Kolmogorov-type differential equations to be solved. The assumption, on which the standard $k-\varepsilon$ model is based, implies that once turbulent energy is generated at the low wave number end of the spectrum, it is dissipated at the high wave number end. In turbulent air flow modelling this is generally the case, because of a vast size disparity between those eddies in which turbulence production takes place, and the eddies in which turbulence dissipation occurs [19]. The standard $k-\varepsilon$ model, examined in this study, employs the eddy viscosity concept and calculates the eddy viscosity using $\nu_t = C_\mu k^2/\varepsilon$. Here the turbulence energy k characterizes the intensity of the turbulent fluctuations and the dissipation rate ε the length scale of the energy-containing eddies through the relation. The distribution of k and ε is determined from the solution of semi-empirical transport equations as in the standard $k-\varepsilon$ model [20], which is summarized in Table 1.

Table 1. Summarized standard $k-\varepsilon$ turbulence model

Equation	Φ	Γ_Φ	S_Φ
T. Kinetic Energy	k	ν_t/σ_k	$\rho(G-\varepsilon)$
Dissipation Rate	ε	ν_t/σ_ε	$\rho(\varepsilon/k)\ (C_{\varepsilon 1}G - C_{\varepsilon 2}\varepsilon$
$G = \nu_t(\partial_k U_i + \partial_i U_k)\partial_k U_i; \nu_t = C_\mu k^2/\varepsilon$			
$(\sigma_k, \sigma_\varepsilon, C_{\varepsilon 1}, C_{\varepsilon 2}, C_\mu) = (1.0, 1.314, 1.44, 1.92, 0.09)$			

The governing equations of the realizable $k-\varepsilon$ turbulence model are,

$$\frac{\partial}{\partial t}(\rho k) + \frac{\partial}{\partial x_j}(\rho k u_j) = \frac{\partial}{\partial x_j}\left[\left(\mu + \frac{\mu_t}{\sigma_k}\right)\frac{\partial k}{\partial x_j}\right] + G_k + G_b - \rho\varepsilon - Y_M + S_k \tag{4}$$

$$\frac{\partial}{\partial t}(\rho\varepsilon) + \frac{\partial}{\partial x_j}(\rho\varepsilon u_j) = \frac{\partial}{\partial x_j}\left[\left(\mu + \frac{\mu_t}{\sigma_\varepsilon}\right)\frac{\partial \varepsilon}{\partial x_j}\right] + \rho C_1 S_\varepsilon - \rho C_2 \frac{\varepsilon^2}{k+\sqrt{\nu\varepsilon}} + C_{1\varepsilon}\frac{\varepsilon}{k} C_{3\varepsilon} G_b + S_\varepsilon \tag{5}$$

where, $C_1 = \max\left[0.43, \frac{\eta}{\eta+5}\right], \eta = S\frac{k}{\varepsilon}, S = \sqrt{2S_{ij}S_{ij}}$ and $S_{ij} = \frac{1}{2}\left(\frac{\partial u_j}{\partial x_i} + \frac{\partial u_i}{\partial x_j}\right)$.

Here G_k represents the generation of turbulence energy due to the mean velocity gradients, G_b is the generation of turbulence kinetic energy due to buoyancy, and Y_M represents the contribution of the fluctuating dilatation in compressible turbulence, to the overall dissipation rate. The model constants are σ_k (=1.0), σ_ε (=1.2), $C_{1\varepsilon}$ (=1.44), C_2 (=1.9). The degree to which ε is affected by the buoyancy is determined by the constant $C_3 = \tanh|v/u|$ where v is the component of the flow velocity parallel to the gravitational vector and u is the component of the flow velocity perpendicular to the gravitational vector. The pollutant dispersion patterns were analysed after solving the

species transport equation, in conjunction with the turbulence model equations. The mass diffusion process was based on the following equations [16, 21],

$$J_i = -\left(\rho D_i + \frac{\mu_t}{Sc_t}\right)\nabla y_i \quad (6)$$

where, J_i is the diffusion flux of the mixture, ρ is the density of the mixture, D_i is the mass diffusion coefficient of the pollutant in the mixture, y_i is the mass fraction of the pollutant, and μ_t is the turbulent viscosity. The turbulent Schmidt (Sc_t) was set at 0.7 - 1.3 [16, 22].

3. Geometry and Boundary Conditions

A 3-dimensional CFD simulation of a generic highway was designed. The atmospheric boundary layer for these studies had neutral boundary condition, The CFD modeled scenario consists of a six-lane divided highway which serves as a source of turbulence and emissions of an inert gaseous tracer with the same density as air. Figure 1 shows a schematic of a section of the computational mesh in the vicinity of double roadside barriers. The mesh was reasonably fine here but was gradually coarsened away from solid surfaces.

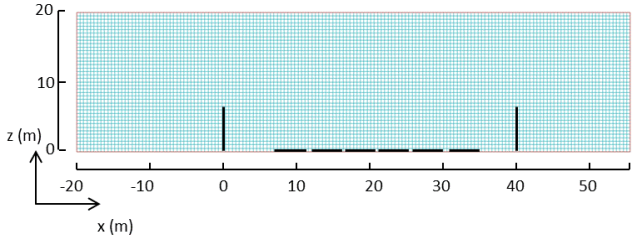

Figure 1. Computational mesh in vicinity of double roadside barriers

Table 2. Single barrier studies

Case	Barrier Height	Wind Speed	Wind Direction
1	0	4 m/s[a]	-
2	H*	4 m/s[a]	90°
3	1.5H	4 m/s[a]	90°
4	H	4 m/s[a]	60°
5	H	4 m/s[a]	30°

[a] Wind speed at height 20H, *H = 6 m

The model for single barriers is oriented with the solid barrier on the downwind side of the roadway, with the model domain extending 800 m downwind of the roadway. In near-road field studies, air pollution impact from major roadways is commonly detected at distances of several hundred meters, although under unique meteorological conditions the spatial extent of near-road air pollution can be up to several kilometers [23]. This model domain is designed to focus on impacts within several hundred meters of a road. For scenarios with perpendicular winds, the model domain is 2000 m along the road axis, 900 m perpendicular to the road, and 200 m in height. The model has a graduated Cartesian mesh, ranging from 0.25 m in close proximity to the barrier and increasing with distance from the road/barrier to 10 m maximum. Multiple model scenarios as given in Table 2, changing barrier height and wind direction, and observing the impact on traffic-related emissions dispersion and resulting near-road air quality were then carried out.

For double barrier studies:

Table 3. Double barrier studies

Case	Barrier Height	Wind Speed	Wind Direction
1	H	12 m/s[b]	90°
2	1.5H	12 m/s[b]	90°

[b]Wind speed at height 83.3H

For the single barrier studies, the modelled scenario matches an existing wind tunnel model [12], in terms of road configuration and atmospheric boundary layer properties. A solid 6 m (1H) high and variations (see Table 2) and 0.5 m thick wall is located along one side of the highway. The barrier height chosen was chosen in part to validate the model against experimental results. There can be found a great variation in barrier heights, depending on, amongst other things, terrain and local wind conditions. It is known, that from a noise reduction point of view that each additional metre in height of barrier above the source/receiver line of sight gives an additional 1.5 dB of noise level reduction [24]. Typical noise barrier ranges from 4 m to 7 m [25]. For the wind tunnel matching simulation, the wall was continuous throughout the domain and located 3.9 m from the nearest lane of traffic. In the CFD simulations that followed, the wall dimensions more closely matched a site where field data have been collected [8] where a 6 m high, 0.5 m thick wall that is located at 5 m from the nearest lane of traffic, and having a discrete length. In the model, the wall spans 750 m of the roadway, with no obstructions to flow for a stretch of the roadway before and after. This design allows changes in the pollutant dispersion due to the barrier to be directly assessed relative to the clearing and also allows the effect of the barrier edges to be observed. A similar computational domain size was used for the double barrier cases, although a different inlet wind profile was chosen as will be detailed below.

The upstream profile was chosen to represent pedestrian-level wind conditions. Much has been written concerning which profile to use. For example [26] proposed inflow boundary conditions of mean wind speed and turbulence quantities for the standard $k-\varepsilon$ model which satisfied the transport equations for k and ε. This is a commonly found boundary condition for wind engineering. Another upstream condition was proposed [27] where again the solution of the turbulence energy equation associated with the standard $k-\varepsilon$ was solved yielding a new set of inflow turbulence boundary conditions.

The inlet boundary condition for u in the neutral boundary condition is,

$$u(z) = \frac{u^*}{k}\ln\left(1+\frac{z}{z_0}\right) \quad (8)$$

where, u^* is the friction velocity, k is the von Karman constant, z_0 is the roughness length and z is the height from the surface. It can be shown [28] that if equilibrium

between turbulence dissipation and production is assumed, the profile for k and ε has the form,

$$(z) = \sqrt{A}\ln(z + z_0 + B \tag{8}$$

where, A and B are constants that can be determined by fitting the equations to the measured profiles of k. Using wind tunnel results [12], for the profile under consideration, $A = -0.075$ and $B = 0.478$ were selected in this study.

Table 4. Boundary conditions

Boundaries	Type	Details
Inlet	Velocity profile	$k = \tau/\rho C_\mu^{1/2}$, $\varepsilon = k^{3/2}C_\mu^{3/4}/l$, $\tau = \rho l^2[\partial u/\partial y]^2$ $u^* = 0.56$ m/s, $z_0 = 0.04$ m
Outlet	Pressure profile	$P = P_{atmos}, k = 0, \varepsilon = 0$
Bottom	Wall	roughness length = 0.25 m
Top	Symmetry	
Left	Symmetry	
Right	Symmetry	
Source	Mass-flow-inlet	Mass-flow-rate = 0.001 kg/s, x,y-velocities = 0, z-velocity =1E-6 m/s
Blockages (Barriers)	No-slip	x,y,z-velocities =0, $k = 0, \varepsilon = 0$

The profile for ε is given by,

$$\varepsilon(z) = \frac{\sqrt{C_\mu}u^*}{k(z+z_0)}\sqrt{A}\ln(z + z_0) + B \tag{9}$$

Table 4 lists the boundary conditions used in this study [29], where the roughness length and friction velocity are those found in [30] and [31] respectively. The composition of NO_x at emission corresponded to 70% NO_2 and 30% NO, and this remained constant over the time and distance modelled. The emission rate of NO_x used was set at 0.222 g/s/km per lane of traffic [32].

4. Results and Discussion

A major part of developing a suitable CFD model suitable to calculate the dispersion of pollutants in the vicinity of solid barriers was the selection of a suitable closure model. As already stated, the $k-\varepsilon$ turbulence model with standard wall functions and the realizable $k-\varepsilon$ turbulence model with various Schmidt numbers (the ratio of the turbulent transfer of momentum in the form of turbulent viscosity to the turbulent transfer of mass in the form of turbulent diffusivity) were used. The role of this important parameter has not been exported extensively within urban areas but values from 0.18 to 1.34 have been suggested in the literature [33]. In this work for wind tunnel comparison values of Sc_t of 0.7, 1.0 and 1.3 were selected. Here, the concentrations of NO_x have been normalized to give the non-dimensional concentration $\chi = CU_rL_xL_y/Q$ [12], where C is the concentration (a fraction by mass) with background concentration subtracted, U_r is the reference wind speed measured at a full-scale equivalent height of 500 m), Q is the mass flow (0.01 kg/s of CO), L_x is along the wind direction of the road (30 m), and L_y is the lateral length of the source segment. As can be seen on Figure 2 the standard and realizable $k-\varepsilon$ turbulence models produce fairly reasonable concentration profiles in the z direction for the 1H barrier case and with X/H = 7. However the standard $k-\varepsilon$ and the realizable $k-\varepsilon$ with Sc_t of 0.7 turbulence models clearly under-predict the ground-level concentration while the realizable $k-\varepsilon$ with Sc_t of 1.3 over-predicts the ground-level concentration. When Sc_t is set to 1, the results are fairly satisfactory. Similar results were found when no barrier was present and when X/H = 20. It was decided therefore, for the rest of the study to use the realizable $k-\varepsilon$ with Sc_t of 1.0. Figure 3 shows a comparison between the calculated and experimental results of surface concentrations at $z = 1$ m height with no barrier present and with $Sc_t = 1.0$. As can be seen a reasonably good comparison was found.

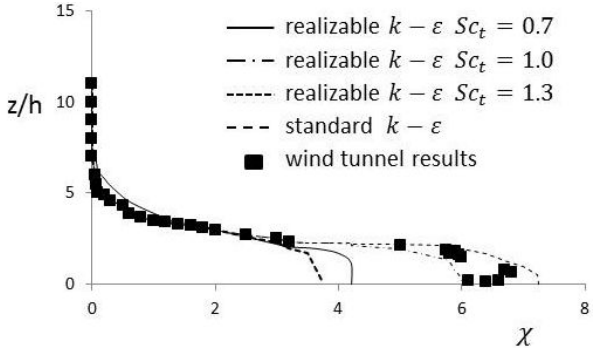

Figure 2. Comparison of wind tunnel and CFD concentration profiles with a barrier of 1H at X/H =7

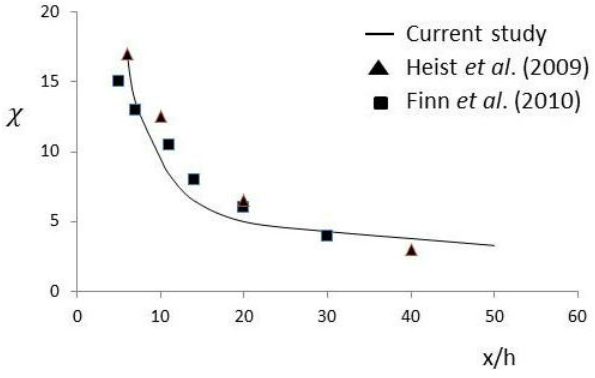

Figure 3. Comparison of experimental and the current simulation model results with no barrier present and at $z = 1$ m

For the single barrier studies, barrier heights of up to 1.5H were modelled to encompass the range of solid barriers commonly used in the urban environment. With winds perpendicular to the roadway, the presence of a barrier leads to vertical lofting of emissions due to an increasing vertical velocity component on the roadway side

of the barrier with increasing height (Figure 4). Also noted on Figure 4 is a recirculating zone downwind of the barrier and this mixing zone extends vertically upwards and slightly exceeds the barrier height. The length of the mixing zone is approximately 10-12 times the barrier height. The gradient of the velocity in the vicinity of the barrier top edge and downwind of the barrier generates turbulent kinetic energy. This increases with barrier height,

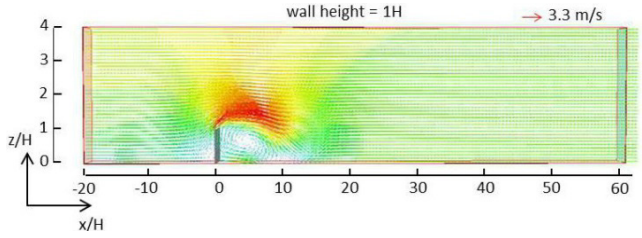

Figure 4. Velocity vectors in the presence of a 1H barrier

After completing the selection of the realizable turbulence model with $Sc_t = 1.0$ a series of flows were calculated for concentration values as detailed in Tables 2 and 3. A simple graduated Cartesian mesh was used throughout these investigations, moving from course to finer meshes for each calculation until the results showed no 'grid dependency'. Typical values for the maximum mesh size for flow with one barrier was around 0.5 million with a resultant CPU time of approximately 8-12 hours.

The vertical lofting of on-road emissions leads to reduced concentrations of NO_x at the ground level, relative to the no-barrier case as shown by the concentration contours of Figure 5. For example, the $\chi = 4$ contours extends further downstream by some 15% for the case with no barrier compared to the 1H barrier calculation.

When the barrier height is increased it would appear that the concentration of NO_x reduces behind the barrier as shown for the case when the barrier height is set at 1.5H. This is in line with experimental finding [12, 13]. However there have been other studies [11, 14] which suggest that roadside barriers may lead to higher pollutant levels at greater distances from the road, when the vertically lofted traffic emissions plume reattaches. This was not found in this model. It can also be seen from these few studies that the vertical concentration profiles are influenced by different barrier heights. Also maximum concentration behind the barrier is reduced with height. Comparing maximum concentrations of NO_x in the near wake of the barriers 1H and 1.5H, reduction of some 40% was found and it is anticipated that this reduction would grow with barrier height.

The majority of current field and wind tunnel results investigating barrier effects on near road air quality focuses on winds perpendicular to the road. The work here extends that analysis to the effect of oblique wind directions (cases 4 and 5 of Table 2). It is especially interesting to understand the effect of the barrier end-points with changing wind direction. Plan views of model results are shown on Figure 6 for concentration contours of χ at 2 m about the ground for wind directions at 60 and 30 degrees to the solid barrier. It can be seen that there are reasonably high concentrations of pollutant downwind of the barrier due to spill-over of accumulated traffic emissions. This spill-over effect has also been noted [8]. It can be seen for the oblique winds that the region of highest near-road concentrations shifts to the far edge of the barrier, while a reduced concentration zone of NO_x appears downwind of the other end of the barrier.

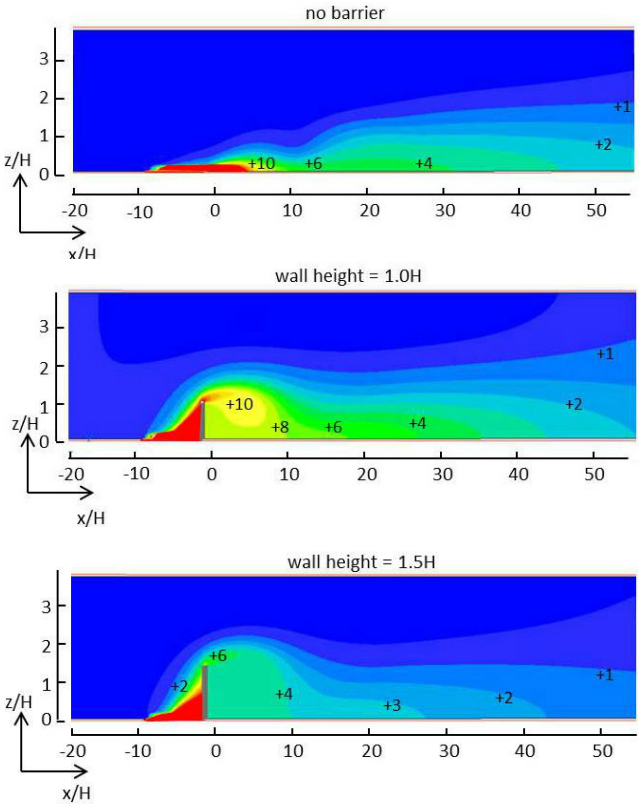

Figure 5. Concentration of NO_x contours (χ) with orthogonal winds for the cases, no barrier, a barrier height of 1H and of 1.5H

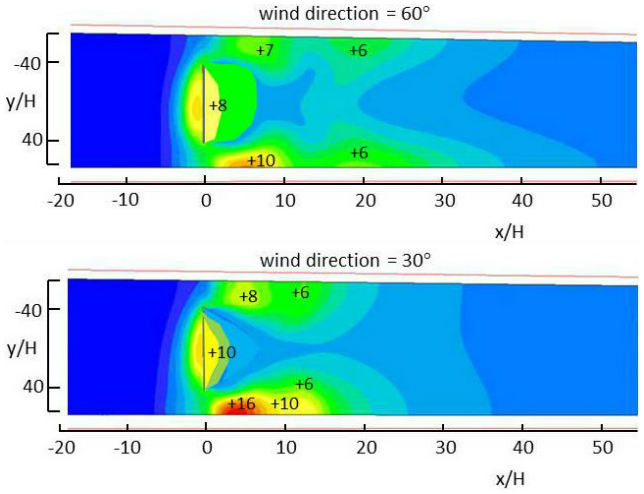

Figure 6. Plan view of concentration of NO_x contours (χ) at 2 m above ground surface with a barrier height of 1H for wind directions of 60° and 30°.

Upwind of the roadside barrier the direction of the

oblique wind affects the on-road concentrations, with less accumulated concentrations being noted with greater angles to the barrier.

Figure 7 shows a typical result for concentration contours (χ) for a double barrier case. The concentration contours for different barrier heights reveal that the double solid barriers height changes the vertical location of maximum concentration, downwind of the road. The presence of a double barrier was found to lead to a vertical lofting of emissions with increasing barrier height. Far wake ground level concentrations were found to reduce with the presence of double barriers relative to the no-barrier case whereas in the near-wake significant air pollution impact from the road traffic was predicted up to 100 - 150 m downwind. This is reasonably in line with experimental findings [34, 23].

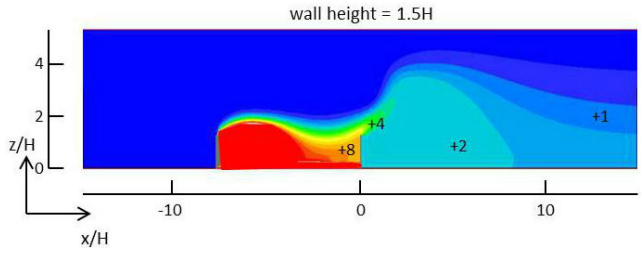

Figure 7. Typical concentration of NO_x contours (χ) for a double barrier for a barrier height of 1.5H

To show the concentration retention of double road barriers, normalized concentrations between the double solid barriers (horizontal distances are from 0 to 40 m) at $z = 1$ m height are shown on Figure 8.

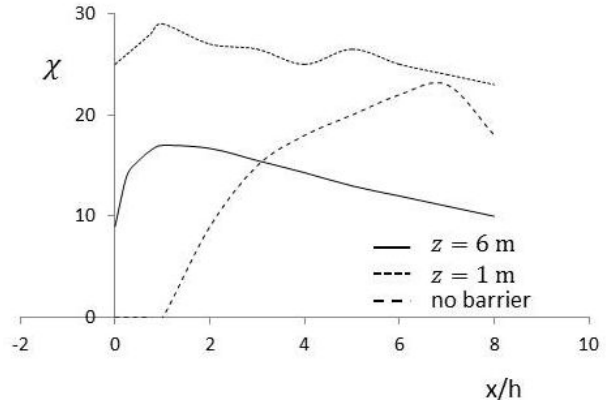

Figure 8. Normalized average concentrations of NO_x between the road barriers at $z = 1$ m and at the barrier top height ($z = 6$ m)

Normalized surface concentrations between the barriers are larger than that of the no barrier case. These increases of normalized concentrations increase with the increase of the solid barrier height. At the top of the barrier however normalized concentration are found to be smaller than those of the surface distribution.

Some results are now given for calculations of NO_x concentrations in terms of $\mu g/m^3$ to facilitate discussion in terms of regulatory aspects. For example, [35] it is generally accepted that nitrogen dioxide should not exceed 200 $\mu g/m^3$ (1 hour mean) more than 18 times per year and 40 $\mu g/m^3$ as the annual mean. It is clear, especially for the double barriers that such low figures would be difficult to achieve in the road area. Taking a height of 1.5 m above the ground, time averages of the horizontal NO_x concentrations distributions with and without barriers are shown on Figure 9. It is very clear that the highest concentrations at this height are found in the road area when two barriers are present and to a lesser extent when one barrier is present, with the peak here moved slightly downwind. When no barrier is present the concentration peak is much lower and moved downwind away from the road area.

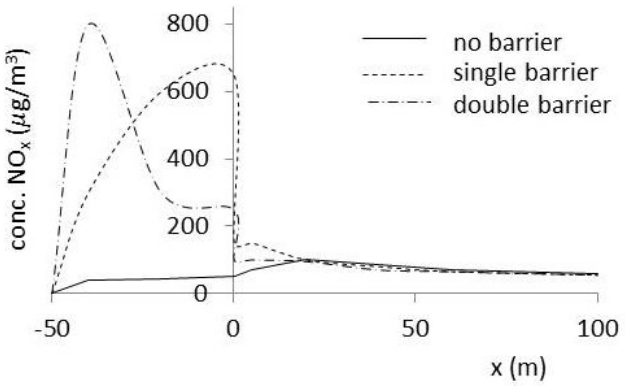

Figure 9. Time averages of the horizontal NOx concentration profiles ($\mu g/m^3$) at a height of 1.5 m above the ground

The distributions are influenced by the recirculation zones behind the barrier and there is some evidence of several maxima over each car lane. Clearly from a regulatory point of view when no barrier exists the concentrations of NO_x are relatively low in the road area but become higher adjacent to the road, possibly causing problems for pedestrians or more importantly residents in that area. Also the value obtained for within the road area is greatly in excess of that proposed by regulatory bodies and during 'rush hours' the limit aspired to could be broken daily.

Vertical profiles of NO_x concentrations, again given in $\mu g/m^3$ are shown on Figure 10 at 10 m from the downwind edge of the highway.

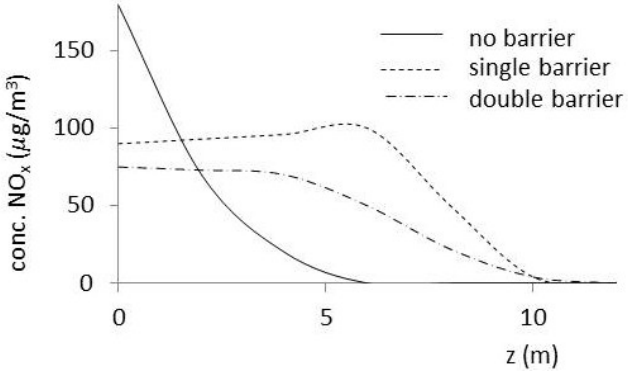

Figure 10. Time averages of the vertical NO_x concentration profiles ($\mu g/m^3$) at 10 m from the downwind edge of the highway.

It can be seen that when barrier(s) are present there is a reduction of in concentration at ground level and an increase in the height at which higher concentrations occur, due to the blocking effect of the barrier and the recirculation behind the barrier. The barriers have the good effect of placing pollution higher in the atmosphere away from pedestrians and residents in their near wakes, with the double barriers more effective than the single barrier.

5. Conclusions

Roadside barriers have many positive uses, including the reduction of noise and aesthetic properties from major traffic corridors in urban regions. This study details the development of a CFD computer model suitable for predicting concentration 'black-spots' of pollution due in part to the position, height and length of these barriers. The realizable $k-\varepsilon$ turbulence model with a Schmidt number of 1.0 was found as the most suitable closure model. Various single and double barrier scenarios were presented with reasonable and plausible results found in comparison to experimental and other simulations found in the literature. It is clear that the presence of barriers has a detrimental effect on the quality of air within the road area but can help with more efficient dispersion downwind of the barriers.

REFERENCES

[1] U. Kenessariyev, A. Golub, M. Brody, A. Dosmukhametov, M. Amrin, A. Erzhanova, D. Kenessary, Human health cost of air pollution in Kazakhstan, Journal of Environmental Protection, Vol. 4, 869-876, 2013.

[2] HEI, Traffic-related air pollution; a critical review of the literature on emissions, exposure, and health effects, HEI special report 17, Boston, MA, Health Effects Institute, 2010.

[3] S. J. Jeong, Effect of double noise-barrier on air pollution dispersion around road, using CFD, Asian Journal of Atmospheric Environment, Vol. 8, No. 2, 81-88, 2014.

[4] H. L. Brantley, G. S. W. Hagler, P. J. Deshmukh, R. W. Baldauf, Field assessment of the effects of roadside vegetation on near-road black carbon and particulate matter, Science of the Total Environment, Vol. 468-469, 120-129, 2014.

[5] J. Stocker, C. Hood, D. Carruthers, C. McHugh, ADMS-Urban: Developments in modelling dispersion from the city scale to the local scale, International Journal of Environment and Pollution, Vol. 50, 308-316, 2011.

[6] N. Kh. Arystanbekova, Application of Gaussian plume models for air pollution simulation at instantaneous emissions, Mathematics and Computers in Simulation, Vol. 67, 451-458, 2004.

[7] Y. F. Zhu, W. C. Hinds, S. Kim, C. Sioutas, Concentration and size distribution of ultrafine particles near a major highway, Journal of the Air & Waste Management Association, Vol. 52, 1032-1042, 2002.

[8] R. Baldauf, E. Thoma, V. Isakov, T. Long, J. Weinstein, I. Gilmour, S. Cho, A. Khlystov, F. Chen, J. Kinsey, M. Hays, R. Seila, R. Snow, R. Shores, D. Olson, B. Gullett, S. Kimbrough, N. Watkins, P. Rowley, J. Bang, D. Costa, Traffic and meteorological impacts on near road air quality: summary of methods and trends from the Raleigh Near Road Study, Journal of the Air & Waste Management Association, Vol. 58, 865-878, 2008.

[9] B. Beckerman, M. Jerrett, J. R. Brook, D. K. Verma, M.A. Arain, M. M. Finkelstein, Correlation of nitrogen dioxide with other traffic pollutants near a major expressway, Atmospheric Environment, Vol. 42, 275-290, 2008.

[10] G. S. W. Hagler, R. W. , Baldauf, E. D. Thoma, T. R. Long, R. F. Snow, J. S. Kinsey, L. Oudejans, B. K. Gullett, Ultrafine particles near a major roadway in Raleigh, North Carolina: downwind attenuation and correlation with traffic related pollutants, Atmospheric Environment, Vol. 43, 1229-1234, 2009.

[11] G. E. Bowker, R. Baldauf, V. Isakov, A. Khlystov, W. Petersen, The effects of roadside structures on the transport and dispersion of ultrafine particles from highways, Atmospheric Environment, Vol. 41, 8128-8139, 2007.

[12] D. K. Heist, S. G. Perry, L. A. Brixey, A wind tunnel study of the effect of roadway configurations on the dispersion of traffic-related pollution, Atmospheric Environment, Vol. 43, 5101-5111, 2009.

[13] D. Finn, K. L. Clawson, R. G. Carter, J. D. Rich, R. M. Eckman, S. G. Perry, V. Isakov, D. K. Heist, Tracer studies to characterize the effects of roadside noise barriers on near-road pollutant dispersion under varying atmospheric stability conditions, Atmospheric Environment, Vol. 44, 204-214, 2010.

[14] Z. Ning, N. Hudda, N. Daher, W. Kam, J. Herner, K. Kozawa, S. Mara, C. Sioutas. Impact of roadside noise barriers on particle size distributions and pollutants concentrations near freeways, Atmospheric Environment, Vol. 44, 3118-3127, 2010

[15] J. T. Steffens, D. K. Heist, S. G. Perry, K. M. Zhang, Modeling the effects of a solid barrier on pollutant dispersion under various atmospheric stability conditions, Atmospheric Environment, Vol. 69, 76-85, 2013

[16] A. Riddle, D. Carruthers, A. Sharpe, C. M. J. Stocker, Comparisons between FLUENT and ADMS for atmospheric dispersion modeling. Atmospheric Environment, Vo. 38, 1029-1038, 2004.

[17] B. E. Launder, D. B. Spalding, The numerical computation of turbulent flows, Computer Methods in Applied Mechanics and Engineering, Vol. 3, No. 2, 269-289, 1974.

[18] T.-H. Shih, W. W. Liou, A. Shabbir, Z. Yang, J. Zhu, A new $k-\varepsilon$ eddy-viscosity model for high Reynolds number turbulent flows - model development and validation, Computers & Fluids, Vol. 24, No. 3, 227-238, 1995.

[19] B. E. Launder, B. Spalding, Mathematical Models of Turbulence, Academic Press, London, 1972.

[20] M. A. Leschziner, W. Rodi, Calculation of annular and twin parallel jets using various discretization schemes and turbulence-model variations, J. Fluids Eng., Vol. 103, No. 2,

352-360, 1981.

[21] W. Y. Ng, C. K. Chau, A modeling investigation of the impact of street and building configurations on personal air pollutant exposure in isolated deep urban canyons, Science of the Total Environment, Vol. 468-469, 429-448, 2014.

[22] S. D. Sabatino, R. Buccolieri, B. Pulvirenti, R. Britter, Simulations of pollutant dispersion within idealized urban-type geometries with CFD and integral models, Atmospheric Environment, Vol. 41, 8316-8329, 2007.

[23] S. S. Hu, S. Fruin., K. Kozawa, S. Mara, S. E. Paulson, A. M. Winer, A wide area of air pollutant impact downwind of a freeway during pre-sunrise hours, Atmospheric Environment, Vol. 43, 541-2549, 2009.

[24] US Department of Transportation, Federal Highway Administration, Noise Barrier Design Handbook, February, 2000.

[25] D. Good, D. Hallden, The design and construction of a noise barrier along the Vanier highway in Fredericton, Conference of the Transportation Association of Canada, Fredericton, New Brunswick, 2012.

[26] P. J. Richards, R. P. Hoxey, Appropriate boundary conditions for computations for computational wind engineering models using the $k-\varepsilon$ model, Journal of Wind Engineering and Industrial Aerodynamics, Vol. 46-47, 145-153, 1993.

[27] Y. Yang, M. Gu, S. Chen, X. Jin, New inflow boundary conditions for modelling the neutral equilibrium atmospheric boundary layer in computational wind engineering, Journal of Wind Engineering and Industrial Aerodynamics, Vol. 97, No. 2, 88-95, 2009

[28] C. Gorle, J. Beeck, P. Rambaud, G. V. Tendeloo, CFD modelling of small particle dispersion: The influence of the turbulence kinetic energy in the atmospheric boundary layer. Atmospheric Environment, Vol. 43, 673-681, 2009.

[29] D. Adair, Numerical calculations of aerial dispersion from elevated sources, Applied Mathematical Modelling, (1990), Vol. 14, 459-467, 1990.

[30] C. S. B. Grimmond, T. S. King, M. Roth, T. R. Oke, Aerodynamic roughness of urban areas derived from wind observations. Boundary-Layer Meteorology, Vol. 89, 1–24, 1998.

[31] J. Hernandez, A. Crespo, Wind turbine wakes in the atmospheric surface layer, PHOENICS Journal, Vol. 3, No.3, 1990.

[32] European Community, Council directive 1999/30/EC of 22 April 1999 relating to limit values for sulphur dioxide, nitrogen dioxide and oxides of nitrogen, particulate matter and lead in ambient air, Official journal of the EC L 163: 0041–0060, 1999.

[33] T. K. Flesch, J. H. Prueger, J. L. Hatfield, Turbulent Schmidt number from a tracer experiment, Agricultural and Forest Meteorology, Vol. 111, 299-307, 2002.

[34] G. S. W. Hagler, W. Tang, M. J. Freeman, D. K. Heist, S. G. Perry, A. F. Vette, Model evaluation of roadside barrier impact on near-road air pollution, Atmospheric Environment, Vol. 45, 2522-2530, 2011.

[35] DEFRA (UK), Local Air Quality Management, Part IV of the Environmental Act 1995, p.A3-12, Department for Environment, Food and Rural Affairs, London, 2009.